

Comparison of Gender Specific and Anthropometrically Scaled Musculoskeletal Model Predictions Using the Sorensen Test

Phillip E. Whitley^(✉), Paulien E. Roos, and Xianlian Zhou

Computational Medicine and Biology Division, CFD Research Corporation,
701 McMillian Way NW, Suite D, Huntsville, AL 35806, USA
{Phil.Whitley, Paulien.Roos, Alex.Zhou}@cfdrc.com

Abstract. Modeling gender and anthropometric influence on human response is essential for understanding biomechanical stressors, population task capability, and injury risk. Arbitrary anthropometric musculoskeletal (MSK) models were generated based on gender and anthropometric variables with MSK muscle strength optimized using lower spinal moment generation capacity. Two female (F1, F2) and two male (M1, M2) MSK models were compared using a 300 s Sorensen test simulation for muscle activation, forces, capacity, pain score, and lumbar joint reaction forces and moments. Predicted muscle activation, force, capacity, pain score, reaction shear and compressive force, and reaction pitch moment followed a body size relationship where $M2 > M1 > F2 > F1$. The anthropometric MSK model generation process created variants that were not simply proportionally scaled versions of the reference model in dimension and strength. The smallest MSK model (F1) exhibited comparatively higher capacity than the other models in agreement with literature.

Keywords: Musculoskeletal models · Anthropometric scaling · Sorensen test · Lumbar model · Anthropometry

1 Introduction

Modeling gender and anthropometric influence on human response is essential for understanding biomechanical stressors, population task capability, and injury risk. We have developed the capability to generate specific, strength-scaled anthropometric musculoskeletal (MSK) models based on gender and anthropometric variables. These scaled MSK models were compared using the Sorensen test.

2 Methods

The anthropometric basis for this effort was a principal component analysis of the ANSUR II survey [1]. New MSK models were created through scaling of a reference 50th percentile gender version of the Christophy et al. [2] lumbar spine model. Starting

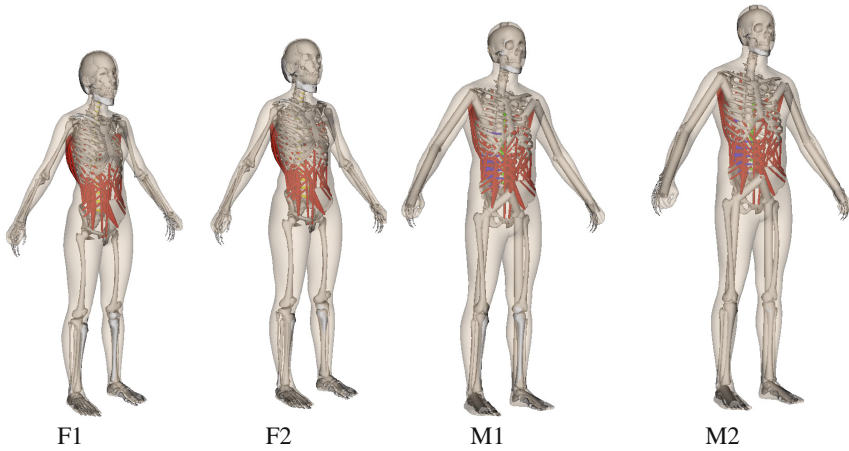


Fig. 1. The four generated models with the musculoskeletal lumbar model shown together with the 3D mesh model.

with specific desired body measurements, the automated process described by Zhou et al. [3] scaled the body habitus, skeletal linkage system and the lumbar vertebral characteristics to those associated dimensions. Male model muscle strength was optimized based on reported lower spinal moment generation capacity of the specified gender associated anthropometry [4–6]. Female model muscle strength was scaled relative to the male model based on Marras et al. [7]. Two female (stature/body mass: F1:1.60 m/49.9 kg and F2:1.68 m/63.3 kg) and two male (stature/body mass: M1:1.78 m/81.5 kg and M2:1.89 m/97.7 kg) MSK models, Fig. 1, were generated for comparison simulation. In the development of this method, the original Christophy model was the basis for scaling but the muscle strength factors were also optimized.

Figure 2 compares the maximum isometric strength about the L3–L4 intervertebral joint for the four generated models.

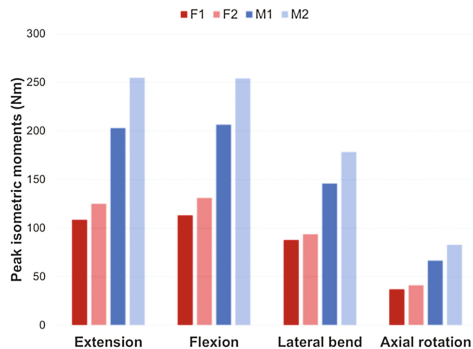


Fig. 2. Comparison of the maximum isometric moment about L3–L4 intervertebral joint for the four generated models.

Capacity – Muscle exertional capacity was predicted using a method reported by Zhou et al. [8]. This semi-empirical muscle force capacity model is an extension of a Hill-type muscle model and is capable of handling the full range of neural excitations (maximal or submaximal) and varying contractile conditions. This model builds on reported muscle fatigue model concepts [9–11] which classify muscle fibers into three mutual exclusive states: resting, activated, and fatigued states. The capacity value range was 0 to 1.

Pain score – A pain score was developed based on the metabolic requirements for muscle exertion and muscle nociceptor response to interstitial metabolites that estimated the potential for the onset of exertional muscle pain. The muscle metabolic model was linked to the musculoskeletal model to predict interstitial concentrations of ATP, Lactate and hydrogen ion (pH) based on muscle demand. The Bhargava et al. phenomenological metabolic model [12] was utilized and represented by linear combinations of different heat/work components further modeled as functions of time, physiological parameters (such as mass fractions of fibers), physical parameters (such as length, mass, etc.), and empirical constants (such as basal heat rates). The skeletal muscle energy consumption was supported by continuous supplies of ATP. The metabolic model predicted the extracellular pH and lactate concentration, but intracellular ATP does not diffuse across the cell membrane due to its molecular size. Rather, ATP is released into the interstitial space when the muscle contracts. Li et al. [13] demonstrated that during contraction tension, muscle releases ATP into the muscle interstitial space in an almost linear fashion related to tension force. A linear curve fit was performed relating the interstitial ATP concentration to the muscle force from this work, which produced a statistically significant ($p < 0.05$), fit with an $r^2 = 0.8$. The regression equation as determined was:

$$[\text{ATP}]_{\text{nM}} = 111 + 36.6 * (\text{Force}) \quad (1)$$

The tension limit range was 0 to 53 N, which yielded an [ATP] from 78 to 1670 nM. The interstitial space concentrations of hydrogen ions, lactate and ATP accumulate and diminish over time, which gives a time course of pain development. Hydrogen ions are rapidly buffered back to a physiological pH and lactate leaves the interstitial space through diffusion into capillaries. However, there are many ways that ATP is utilized in the muscle interstitial space. The accumulation and utilization of ATP in the model was estimated through a general first-order response with a time constant of 200 s to approximate the combined effects of extracellular ATP half-life [14, 15], subjective pain response [16] and subjective pain duration [17].

A synergistic relationship has been demonstrated for subjective muscle pain response between hydrogen ions, ATP and Lactate, which was used to calculate a pain score [17, 18]. A response surface regression equation was fit to these subjective data as a function of their study pH, ATP and Lactate levels and is given below:

$$\begin{aligned} \text{Pain Score} = & -65.451 + 18.943(\text{pH}) + 0.001(\text{ATP}) + 0.007(\text{LAC}) - 1.365(\text{pH})^2 - 6.95\text{E} - 08(\text{ATP})^2 \\ & + 4.256\text{E} - 05(\text{LAC})^2 - 0.0001(\text{pH})(\text{ATP}) - 0.0008(\text{pH})(\text{LAC}) \\ & + 1.126\text{E} - 06(\text{ATP})(\text{LAC}) \end{aligned} \quad (2)$$

Where the final model $r^2 = 0.873$, ($p < 0.001$) and muscle interstitial values are: (pH) in pH units, (ATP) is the concentration of ATP in nM and (LAC) is the concentration of mM. The Pain Score range is limited to 0 to 1. The estimated pH, ATP and Lactate metabolite levels with respect to exercise level [17] were compared to the calculated pain score shown in Table 1.

Table 1. Major metabolite levels, exercise level and predicted pain score.

pH	ATP (nM)	Lactate (mM)	Exercise level	Pain score
7.4	300	1	Resting	0.06
7.3	400	4	Mild	0.22
7.2	500	10	Moderate	0.36
7.0	1000	15	High	0.64
6.8	2000	20	Very high	0.92
6.6	5000	50	Ischemic	1.0

2.1 Comparison of Anthropometric Model Performance

The four anthropometric models were compared using the Sorensen Test. Figure 3 shows the Sorensen test configuration [19] and an oblique view during simulation of the test.

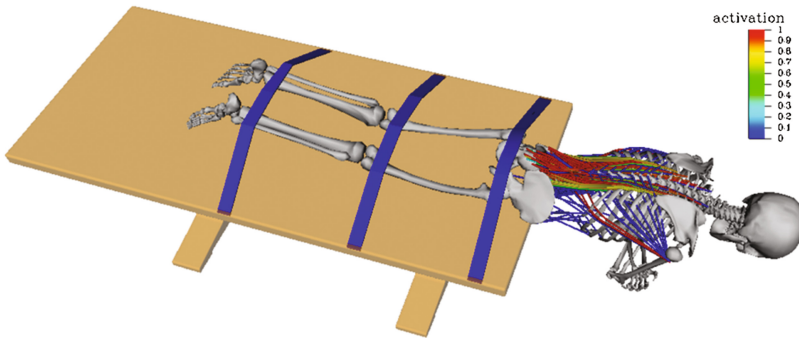


Fig. 3. Sorensen test simulation with muscle activation.

In the Sorensen test, the subject holds their unsupported torso in a horizontal position while the lower body is strapped to a table. The simulation duration was 300 s, approximately twice the normative test value. The simulation predicted muscle activation, forces, capacity, and a pain score along with joint reaction forces and moments at the lumbar functional spinal unit level.

3 Results

The muscle data results were compared across the anthropometric models for the left side. The left and right side muscle results were equivalent across all anthropometric models. Group results were average values across all fascicles within the longissimus thoracis pars lumborum (LTpL) and iliocostalis lumborum pars thoracis (ILpT). The comparisons of the LTpL and ILpT group average activation, force, capacity and pain score are shown in Figs. 4, 5, 6, and 7, respectively.

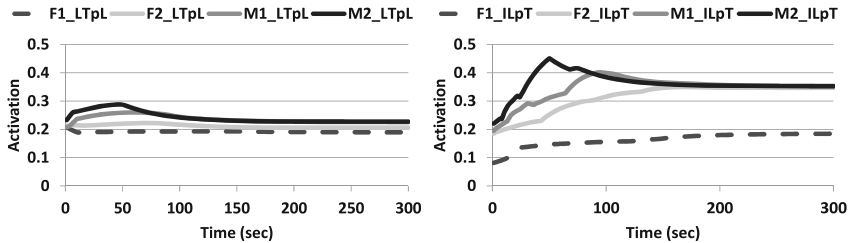


Fig. 4. Group average muscle activation comparisons.

The group average activation results in Fig. 4 show that the ILpT exhibits greater activation than the LTpL. The muscle activation is the fraction of available muscle force contraction employed. Initial activation followed model size variation with the largest model showing the highest activations. While the LTpL reaches asymptotic activation by approximately 100 s, the ILpT required approximately 150 s to reach an asymptote.

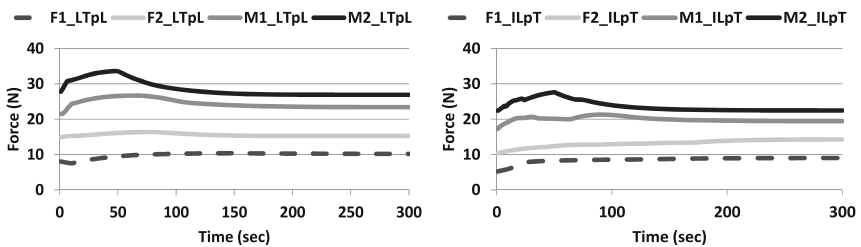


Fig. 5. Group average muscle force comparisons.

LTpL and ILpT group muscle average force comparisons are shown in Fig. 5. As the activation values show the fraction of full muscle contraction force, the actual force predictions show the LTpL generated higher forces compared to the ILpT. Again the force magnitudes are related to the anthropometric model size where the large male (M2) shows the higher forces followed by M1, F2, and F1.

Figure 6 shows the ILpT and LTpL average group capacities. The muscle capacity is an indicator of the muscle fatigue over time. The ILpT capacity approaches 0.75 for

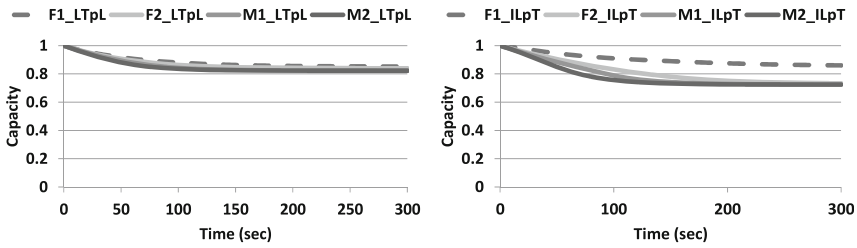


Fig. 6. Group average muscle capacity comparisons.

M2, M1 and F2, but the LTpL capacity is above 0.8 in all cases (lower activation). The ILpT capacity loss follows a body size relationship over the first 100–150 s, except for the F1 model, which shows a minimal capacity decrease.

The LTpL and ILpT average group pain scores are shown in Fig. 7. The ILpT and LTpL exhibit an increase in pain score over time. The pain score time histories show a body size relationship where M2 shows the highest score followed by M1, F2 and then F1. Pain scores of approximately 0.3 would be consistent with just below moderate exercise exertion.

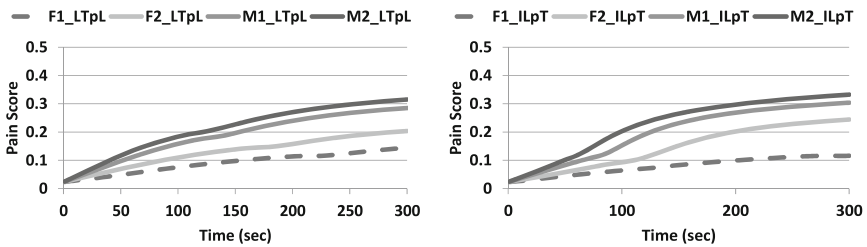


Fig. 7. Group pain score comparisons for erector spinae muscles.

3.1 Intervertebral Disc Joint Reaction Data

The maximum reaction forces and moments for the intervertebral disc (IVD) joints of the lumbar spine are shown in Figs. 8, 9, and 10. The forces in the x direction (back to front, shear), F_x , are shown by vertebral level and anthropometric model in Fig. 8. The highest shear forces are seen at the L2_L3 level followed by L3_L4.

The reaction shear forces at L4_L5, L3_L4, L2_L3, and L1_L2 follow a body size relationship where M2 exhibits the highest force followed by M1, F2 and then F1. The reaction shear forces at L5_S1 follow the same size relationship except for F1 and F2, which are approximately the same shear force. While the F_x time history (not shown) peaks at approximately 60 s for M2 and M1 at all vertebral levels, this peaking response is not seen for either female model.

The forces in the y direction (vertical, compression), F_y , are shown by vertebral level and anthropometric model in Fig. 9. The highest compressive forces were seen at L5_S1 followed by L4_L5 with the other levels close behind showing a similar response.

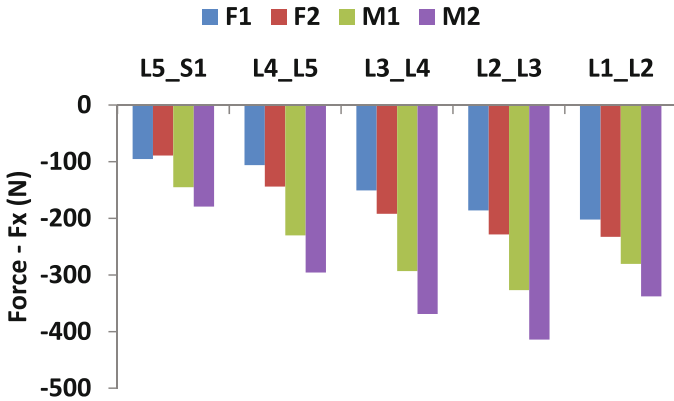


Fig. 8. IVD reaction force Fx by vertebral level and anthropometric model.

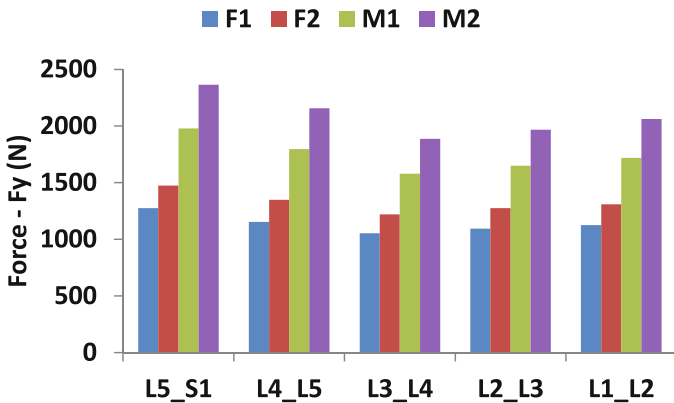


Fig. 9. IVD reaction force Fy by vertebral level and anthropometric model.

A body size relationship was observed with respect to compressive forces. The same force time history peaking response was observed in compression (not shown) in the male models but not in the female models.

The forces in the z direction (lateral shear), Fz, as well as the lateral and axial moments, Mx and My, were extremely small owing to the symmetry of the simulated task and the optimized model performance and were not reported.

The reaction moment about the z direction (pitch), Mz, are shown by vertebral level and anthropometric model in Fig. 10. The highest moments are seen at L5_S1, which are almost double of that at the next highest vertebral level L4_L5. The moments by model show a decrease from L3_L4 to L2_L3 but then and increase from L2_L3 to L1_L2, likely due to the maintenance of the lumbar lordosis by the spinal model constraint.

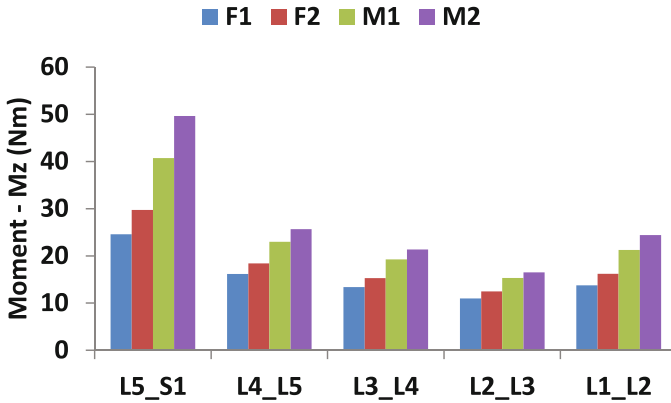


Fig. 10. IVD reaction moment M_z by vertebral level and anthropometric model.

4 Discussion and Conclusions

The anthropometric MSK model generation process created specific variants that were not simply proportionally scaled versions of the reference MSK model in dimension. The predicted results indicate the importance of strength scaling when generating a scaled anthropomorphic model. The differences between the anthropometric models results are related to the variation in back muscle strength as well as the torso mass and moment arm variation by anthropometry. The smallest MSK model (F1) results were notably lower than the other models but studies indicate that females exhibit significantly longer holding times than males [19]. The IVD reaction forces and moments for the Sorensen test follow a body size relationship. Given the nature of the simulated task, sagittal plane moments were significant while minimal transverse or coronal plane moments were observed. While lateral forces were minimal, significant shear and compressive forces by level and significant sagittal plane (extension) moments were observed. Variations by vertebral level for reaction compression and shear as well as sagittal plane moment follow a pattern with change noted in the L3_L4 to L2_L3 region where a parameter reaches a peak or a valley in this region. This pattern is likely due to lumbar lordosis and the model’s maintenance of lordosis by the spinal model constraint. The MSK generation approach and predicted results will be further validated through graded Sorensen tests with human volunteers.

References

- Gordon, C.C., Blackwell, C., Bradtmiller, B., Parham, J., Barrientos, P., Paquette, S., Corner, B., Carson, J., Venezia, J., Rockwell, B., Mucher, M., Kristensen, S.: 2012 Anthropometric Survey of U.S. Army Personnel: Methods and Summary Statistics. NATICK TR-15/007 (2014)

2. Christophy, M., Faruk Senan, N., Lotz, J., O'Reilly, O.: A Musculoskeletal model for the lumbar spine. *Biomech. Model. Mechanobiol.* **11**, 19–34 (2012)
3. Zhou, X., Sun, K., Roos, P., Li, P., Corner, B.: Anthropometry model generation based on ANSUR II database. *Int. J. Digit. Hum.* **1**(4), 321–343 (2016)
4. Kumar, S.: Isolated planar trunk strengths measurement in normals: part III — results and database. *Int. J. Ind. Ergon.* **17**, 103–111 (1996)
5. Kumar, S., Dufresne, R.M., Garand, D.: Effect of body posture on isometric torque-producing capability of the back. *Int. J. Ind. Ergon.* **7**, 53–62 (1991)
6. Larivière, C., Gravel, D., Gagnon, D., Bertrand Arsenault, A., Loisel, P., Lepage, Y.: Back strength cannot be predicted accurately from anthropometric measures in subjects with and without chronic low back pain. *Clin. Biomech.* **18**, 473–479 (2003)
7. Marras, W.S., Jorgensen, M.J., Granata, K.P., Wiand, B.: Female and male trunk geometry: Size and prediction of the spine loading trunk muscles derived from MRI. *Clin. Biomech.* **16**, 38–46 (2001)
8. Zhou, X., Whitley, P., Przekwas, A.: A musculoskeletal fatigue model for prediction of aviator neck manoeuvring loadings. *Int. J. Hum. Factors Model. Simul.* **4**, 191–219 (2014)
9. Liu, J.Z., Brown, R.W., Yue, G.H.: A dynamical model of muscle activation, fatigue, and recovery. *Biophys. J.* **82**, 2344–2359 (2002)
10. Xia, T., Frey Law, L.A.: A theoretical approach for modeling peripheral muscle fatigue and recovery. *J. Biomech.* **41**, 3046–3052 (2008)
11. Frey-Law, L.A., Looft, J., Heitsman, J.: A three-compartment muscle fatigue model accurately predicts joint-specific maximum endurance times for sustained isometric tasks. *J. Biomech.* **45**, 1803–1808 (2013)
12. Bhargava, L.J., Pandey, M.G., Anderson, F.C.: A phenomenological model for estimating metabolic energy consumption in muscle contraction. *J. Biomech.* **37**, 81–88 (2004)
13. Li, J., King, N.C., Sinoway, L.I.: ATP concentrations and muscle tension increase linearly with muscle contraction. *J. Appl. Physiol.* **95**, 577–583 (2003)
14. Gündüz, D., Kasseckert, S.A., Härtel, F.V., Aslam, M., Abdallah, Y., Schäfer, M., Piper, H.M., Noll, T., Schäfer, C.: Accumulation of extracellular ATP protects against acute reperfusion injury in rat heart endothelial cells. *Cardiovasc. Res.* **71**, 764–773 (2006)
15. Clemens, M.G., Forrester, T.: Appearance of adenosine triphosphate in the coronary sinus effluent from isolated working rat heart in response to hypoxia. *J. Physiol.* **312**, 143–158 (1981)
16. Arendt-nielsen, L., Graven-nielsen, T.: Muscle pain: sensory implications and interaction. *Clin. J. Pain* **24**, 291–298 (2008)
17. Pollak, K.A., Swenson, J.D., Vanhaisma, T.A., Hughen, R.W., Jo, D., White, A.T., Light, K.C., Schweinhardt, P., Amann, M., Light, A.R.: Exogenously applied muscle metabolites synergistically evoke sensations of muscle fatigue and pain in human subjects. *Exp. Physiol.* **99**, 368–380 (2014)
18. Light, A.R., Hughen, R.W., Zhang, J., Rainier, J., Liu, Z., Lee, J.: Dorsal root ganglion neurons innervating skeletal muscle respond to physiological combinations of protons, ATP, and lactate mediated by ASIC, P2X, and TRPV1. *J. Neurophysiol.* **100**, 1184–1201 (2008)
19. Demoulin, C., Vanderthommen, M., Duysens, C., Crielaard, J.-M.: Spinal muscle evaluation using the Sorensen test: a critical appraisal of the literature. *Joint Bone Spine* **73**, 43–50 (2006)